Search for TeV Gamma-Rays in Gamma-Ray Bursts with the L3+Cosmics detector

M. van den Akker

23 January 2003

Abstract

We have investigated the possible presence of highly energetic (TeV) gamma-rays correlated with Gamma-Ray Bursts (GRBs) measured at 100 keV energies by CGRO-BATSE. Observation of TeV gamma-rays is done indirectly by searching for muons initiated by such highly energetic photons in atmospheric particle cascades using the L3+Cosmic experiment at CERN. During the active period of the L3+Cosmics experiment 8 GRBs, that were detected by CGRO-BATSE, were in the field of view of the detector. Three methods have been used to look for high energy signals from these bursts during a period of one hour coinciding with the GRB. First a search for significant excess above background using different sampling times is performed. Next, lightcurve information from CGRO-BATSE is correlated with the muon data. Finaly an analysis over a 24 hour period is done. Neither method shows a significant muon excess compared to the muon background. From these analyses we obtain an upper limit for the TeV gamma-ray flux of $S_\gamma \leq 3.36 \cdot 10^{-3}$ erg cm^{-2} s^{-1} for the investigated bursts.

1 Introduction

Gamma-ray bursts (GRBs) are short bursts of photons in which most of the energy is emitted in the sub-MeV band ($\sim$ 100 keV). The bursts are distributed isotropically and are now known to originate (at least partly) in star forming regions of galaxies [1, 2]. Although their existence has been known for 30 years [3] they still remain one of the most mysterious astronomical phenomena. One of the reasons is that GRBs have been observed mostly in the soft gamma-ray band. A lot of progress has been made after the discovery of afterglows in the X-ray, optical and radio bands [1].

For a better understanding of GRBs it is also important to search for gamma-rays beyond the sub-MeV band. Measurements of the gamma-ray flux at energies beyond 30 GeV are not feasable for satellite borne experiments due to their small detector areas. The large detector that area needed to detect these high energetic sources are only available at ground-based experiments. These high-energetic photons create an extensive air shower that can be detected at ground level by detecting the Cherenkov light of the cascading relativistic particles or by detecting the particles that reach ground level.

Although Cherenkov telescopes have a large collection area ($\sim 10^5$ m^2) and are good in rejecting hadronic events they have a small opening angle (a few degrees) and can only operate on dark and clear nights. This makes them ill suited to search for transient sources such as GRBs.

A search for GRBs above 20 TeV was done by the HEGRA AIROBICC Cherenkov array. Two GRBs occurred within their field of view, but no claim for a firm detection could be made [4].

In the early 90's the Tibet air shower array did find some burst like events coinciding with BATSE bursts, but due to their large positional error a convincing claim for a signal could not be made. Superposition of all observed bursts resulted in a 6σ deviation from background [5].

Measurements with the Milagrito detector show that from the 54 GRBs that were in the field of view, only one (GRB 970417a) showed an excess in space and time [6].

In this paper we present the results of the search for TeV emission of GRBs using the L3+Cosmics detector at CERN. Observation of TeV gamma-rays is done indirectly by looking for muons initiated by such highly energetic photons in atmospheric particle cascades.

After a description of the criteria for the GRB and event selection we describe two methods used in this analysis. The first method is used to look for the maximum

deviation from the muon rate during a 1 hour time span around GRB active period. The second method correlates the lightcurve information of the GRBs with the muon data. Finally we give an estimate of the gamma-ray flux limit.

2 Event selection

2.1 GRB event selection

The position and time at which a GRB occured is obtained from the GRB Coordinate Network (GCN) web site [7] which contains all relevant information about any given burst in a single location. This information is obtained using CGRO-BATSE and other spacecraft instruments like RXTA-PCA, RXTE-ASM, CGRO-COMPTEL, Beppo-SAX and Ulysses through the Interplanetary Network (IPN) [8].

From the GCN catalog only those GRBs are selected that satifsfy the following criteria:

- The burst occurs in the period 1 August 1999 – 9 November 1999 or 31 March 2000 – 12 November 2000. This is the period in which L3+C was properly taking data.
- The position at which the GRB takes place corresponds to an altitude of at least 30° above the horizon at the L3+C site. This ensures that the GRB is within the field of view of the detector.
- Data acquisition has to be active for at least 95% of the time during the period from 30 minutes before until 30 minutes after the GRB trigger. Here we assume that the TeV part of the GRB signal wil arrive within 30 minutes of the keV signal.

Applying these criteria results in the selection of eight GRBs, listed in Table 1. Even though data from various instruments (CGRO-BATSE, Beppo-SAX and Alexis) were used, the triggers for all the selected GRBs originate from CGRO-BATSE. The decommisioning of the Compton Gamma-Ray Observatory (CGRO) on 27 May 2000 resulted in the selection of only three GRB candidates for that year.

2.2 Muon event Selection

Reconstructed events of high quality are required to accurately point to a specific area in the sky. The event selection criteria herefor are listed below.

Table 1: List of the selected GRBs that are within the field of view of L3+Cosmics

Name / Date (yymmdd)	UT[a] GRB trigger	RA (deg.)	δ (deg.)	Azimuth[b] (deg.)	Altitude (deg.)	Uncertainty[c] (deg.)
GRB 990903	$19^h14^m56^s$	345.22	73.66	24.04	50.18	2.1
GRB 990917	$20^h12^m28^s$	324.60	16.65	145.57	56.23	1.8
GRB 991025	$16^h56^m30^s$	257.21	44.02	278.01	64.36	0.7
GRB 991103	$18^h42^m41^s$	320.84	15.22	195.48	57.99	2.7
GRB 991106	$19^h3^m32^s$	39.30	60.60	44.99	52.13	0.9
GRB 000403	$13^h33^m2^s$	57.22	24.68	144.52	64.85	3.5
GRB 000415	$0^h16^m10^s$	175.59	68.32	332.11	60.95	8.7
GRB 000424	$18^h18^m8^s$	105.07	53.96	303.00	70.40	0.9

[a]Universal Time
[b]Calculated Eastward, starting from the North.
[c]1σ uncertainty in the detected position of the GRB by satellite observations

- An event must consist of only one track. This removes the multi-muon events that are mainly created by hadrons;
- The energy of the muon at surface level has to be at least 30 GeV. Lower energy will decrease the pointing precision due to multiple scattering in the molasse. This gives an uncertainty in the direction of 1°;
- The reconstructed muon track has to be built up from at least 1 P-triplet and 1 Z-doublet. The P-triplet is formed from sub tracks in the MI, MM and MO layers that have to contain at least 8, 12 and 8 hits respectively.

2.3 Angular and temporal selection

As we try to keep the measurement conditions as constant as possible, we select a fixed area of the sky (zenith and azimuthal angle are kept constant) around the GRB position. This position is monitored for a 1 hour period in which the GRB occurs in this area, starting 30 minutes before the GRB trigger and ending 30 minutes after the GRB trigger. Because of the rotation of the earth, the GRB will move through this monitored area at a rate of $15 \times \cos(\delta)$ degrees per hour, where δ is the declination of the GRB. The duration of the bursts in the keV regime, is in the order of seconds for all selected bursts. Assuming that this will not be larger for a possible burst in the

TeV regime, the movement of the GRB during the burst is negligible.

The size of the monitored area is based on the following points:

- The uncertainty in the location of the burst (as given in the last column of Table 1) is, except for GRB000415, three degrees or less;
- The displacement of the source in a 30 minute period. This corresponds to 5° for a source at $\delta = 50°$.
- Deviation of the muon direction from the primary photon direction. Most of the muons produced in photon induced showers (75%) are within 1° of the direction of the primary [9].
- Due to multiple scattering an additional uncertainty of 1° is added to the total uncertainty in the direction of the source.

Although a larger monitoring area increases the possibility of containing the burst, it also increases the number of background events and is therefore not favoured. Taking all these points into account a circular area with a radius of 5° was chosen.

3 Analysis

3.1 Sampling Time Optimization

The duration of the selected GRBs in the keV regime is in the order of a few seconds. Assuming that the duration of a burst in the keV regime is the same as in the TeV regime, the same time scale has to be chosen for the sampling time t_{samp}. If t_{samp} is too large, the signal will disappear in the background whereas a t_{samp} that is too small will result in a signal that is distributed over multiple bins in time.

During our signal search we optimize t_{samp} such that a muon rate is found that has the smallest probability of being caused by a fluctuation in the muon background. First, the data is sampled at 1.024 second intervals which is the same sampling frequency as used for the CGRO-BATSE lightcurve information which will be used in section 3.2.

The data is then rebinned trying various values of t_{samp}, ranging from 2.048 to 20.48 seconds with steps of 1.024 seconds. This range covers the timescales of the 8 selected bursts as observed in the sub-MeV regime. The rebinning introduces a new parameter, namely the offset position where the rebinning starts. Therefore we first have to determine an optimized value for this parameter. For a sampling time of

$t_{\rm samp} = m \times 1.024$ seconds this is done by calculating, for each time t_i, the number of muons in m consecutive time bins,

$$M(t_i) = \sum_{j=i}^{i+m-1} \mu(t_j), \tag{1}$$

where $\mu(t_j)$ is the number of muons at time t_j. The offset position is chosen to be the time where $M(t_i)$ is maximal.

After rebinning, the muon background is estimated from the average muon rate and it is used to calculate the probability that the measured muon rate corresponds to a fluctuation in the muon background. For a sampling time of $m \times 1.024$ seconds, the smallest probability found is called P_m.

If we define $m_{\rm opt}$ as the value of m for which P_m is minimal then the optimized sampling is defined as $t_{\rm samp} = m_{\rm opt} \times 1.024$ seconds.

The results of the method described above for the selected eight GRBs can be seen in figures 1 to 8. The numerical values of the relevant parameters are listed in table 2. The column $E(r \geq r_{\rm max}|\langle R \rangle)$ represents the estimated number of time bins with a muon rate r that is equal or larger than the maximum observed muon rate $r_{\rm max}$. $P(n \geq n_{\rm max}|E)$ is the probability that the number of bins with $r \geq r_{\rm max}$ is larger than the number of bins which have the maximum observed rate $n_{\rm max}$. For all GRBs that are investigated, $n_{\rm max} = 1$.

The peak value that is found for GRB990917 at $t - t_{\rm GRB} = 500\,{\rm s}$ occurs just before the start of a new LEP run and is therefore likely to be caused by LEP during beam preparation.

We also note that the majority (6 out of 8) of the peaks that are found occur before the GRB trigger.

A similar analysis was done 1 hour before the GRB trigger with the GRB outside the field of view. The result of this is listed in table 3. Also for these measurements we have $n_{\rm max} = 1$.

The 90% confidence level for the upper limit, listed in table 2, is obtained by using the unified approach as described by Feldman and Cousins [11]. Assuming that all the excesses we see are caused by fluctuations in the muon background we get upper limits for the muon rate for the 8 GRBs investigated ranging from 0.75 up to 9.62 muons per second.

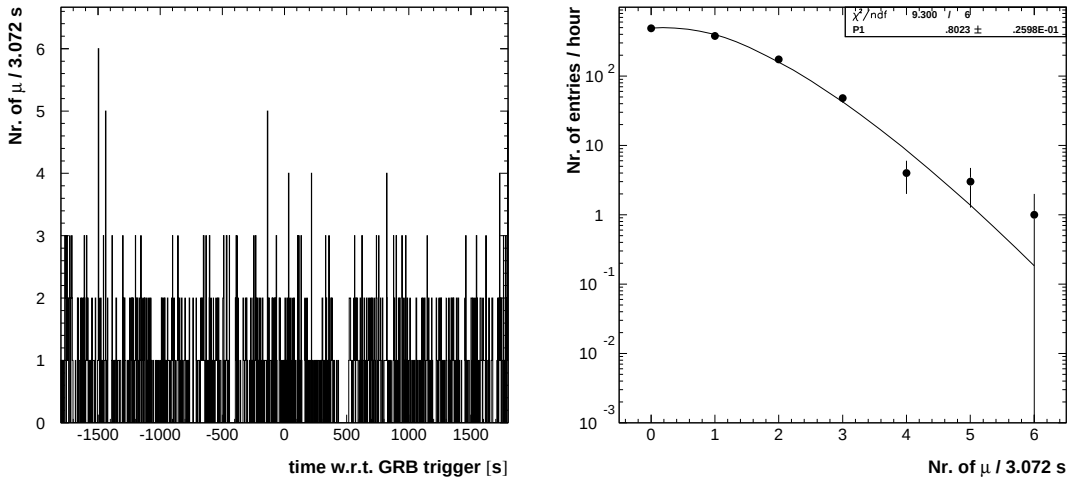

(a) (b)

Figure 1: (a) Muon rate versus time for GRB990903. (b) Corresponding distribution.

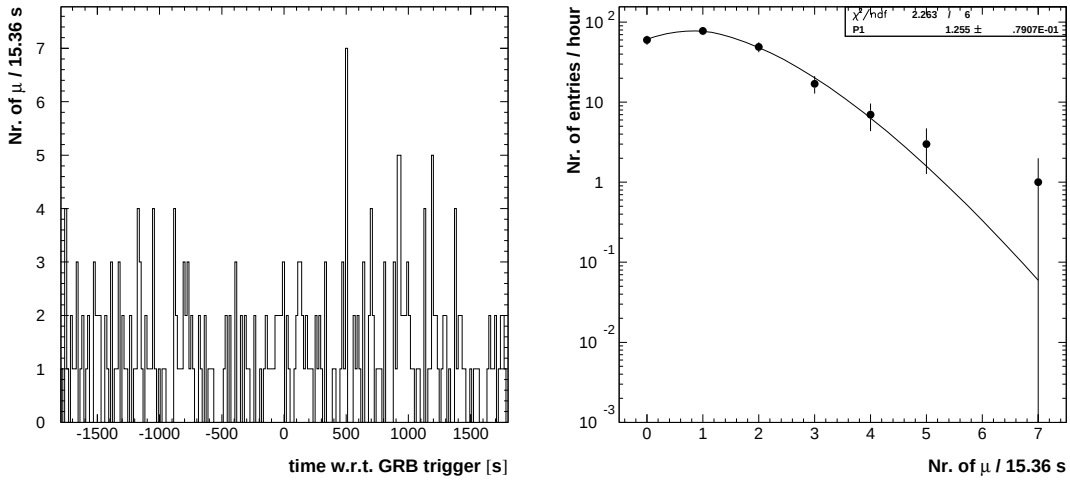

(a) (b)

Figure 2: (a) Muon rate versus time for GRB990917. (b) Corresponding distribution.

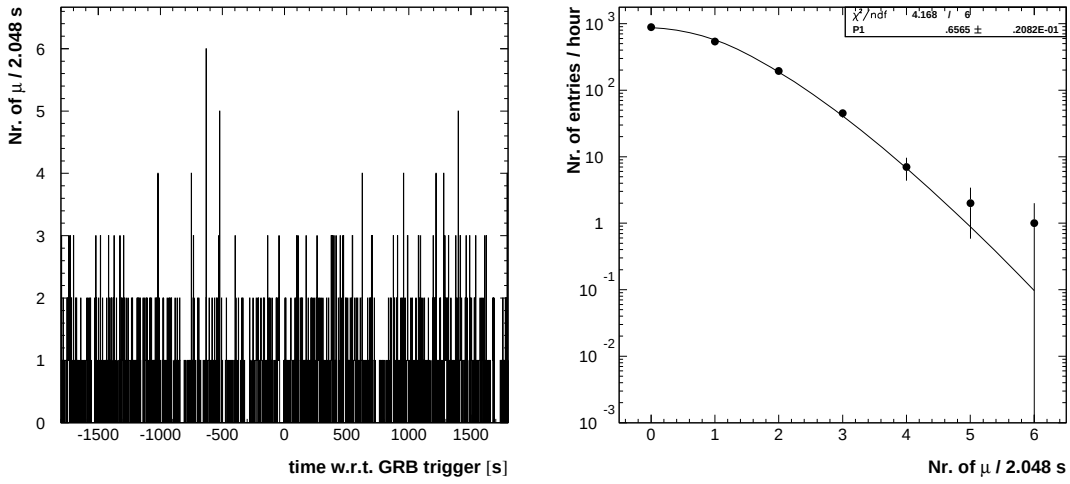

(a) (b)

Figure 3: (a) Muon rate versus time for GRB991025. (b) Corresponding distribution.

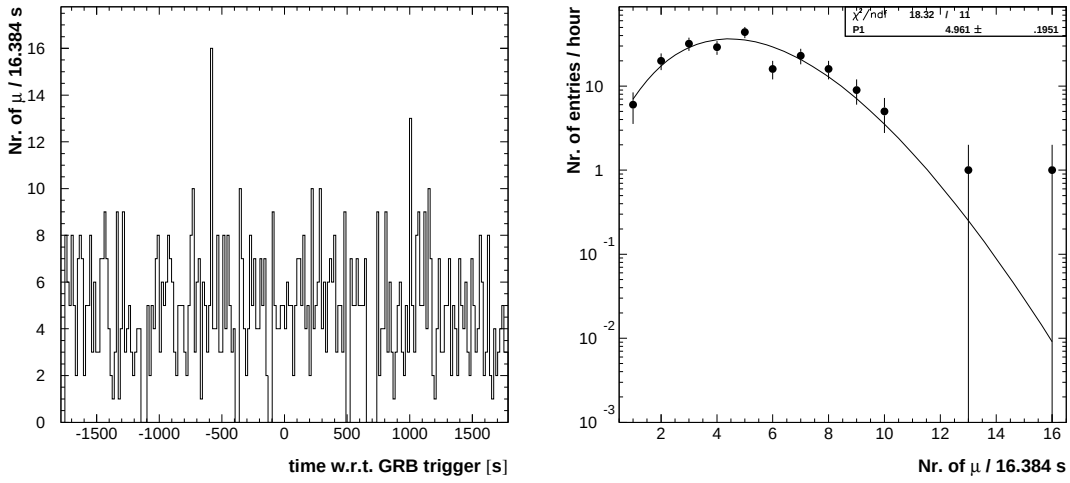

(a) (b)

Figure 4: (a) Muon rate versus time for GRB991103. (b) Corresponding distribution.

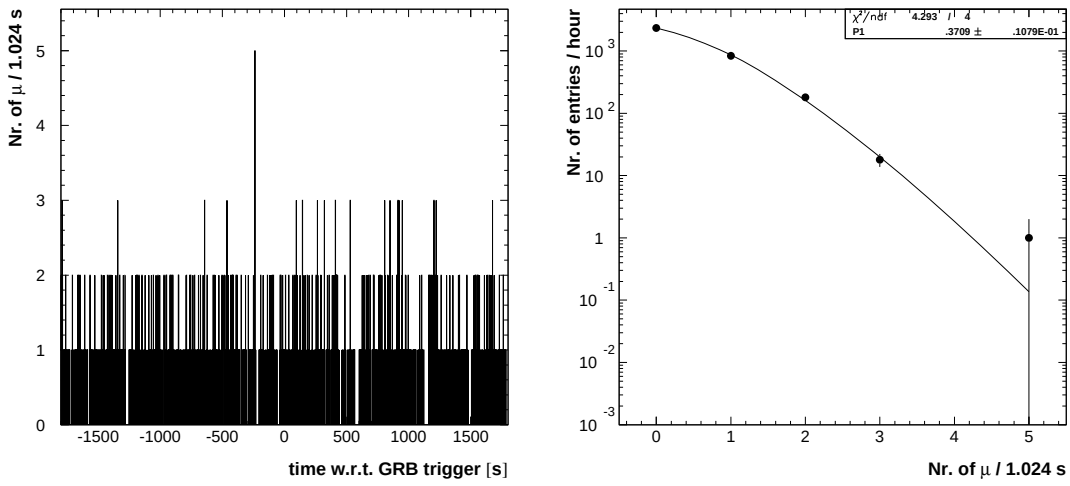

(a) (b)

Figure 5: (a) Muon rate versus time GRB991106. (b) Corresponding distribution.

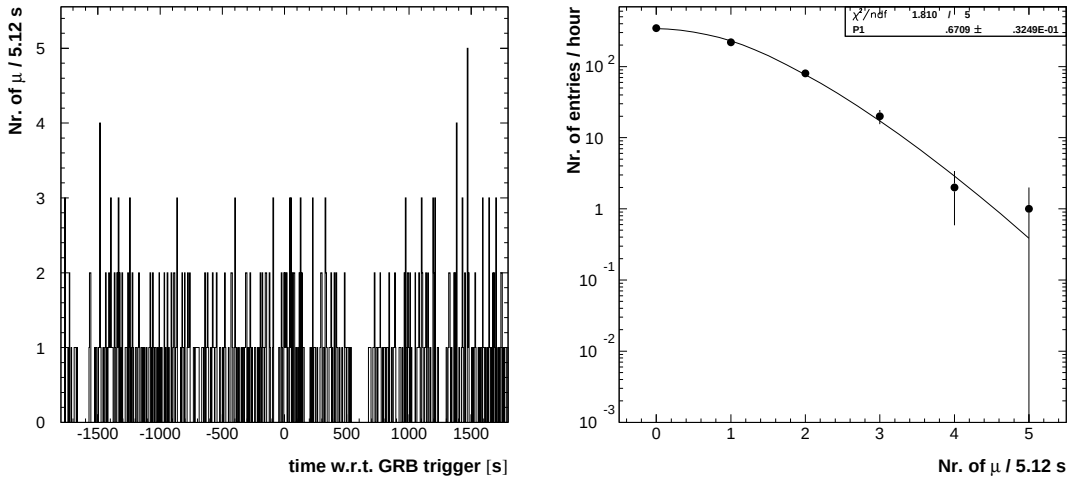

(a) (b)

Figure 6: (a) Muon rate versus time for GRB000403. (b) Corresponding distribution.

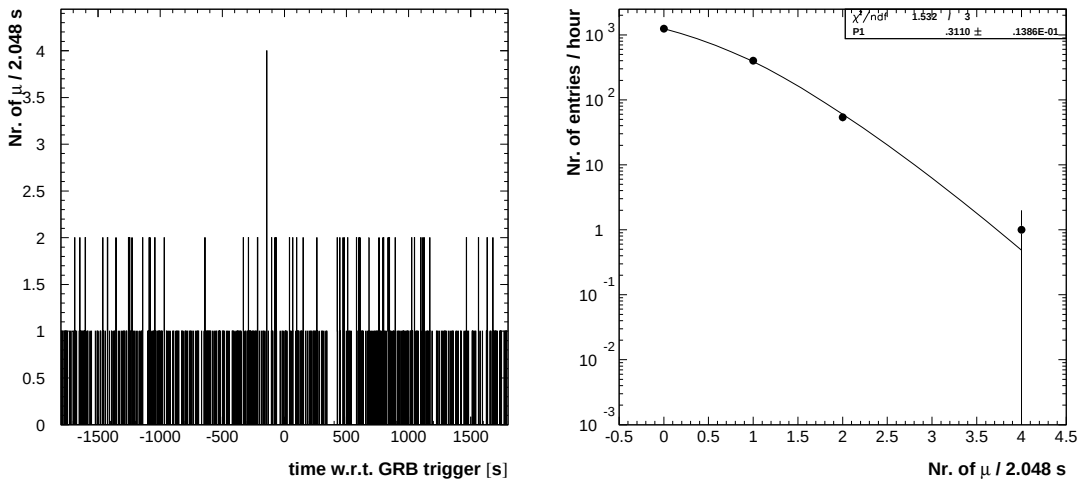

(a) (b)

Figure 7: (a) Muon rate versus time for GRB000415. (b) Corresponding distribution.

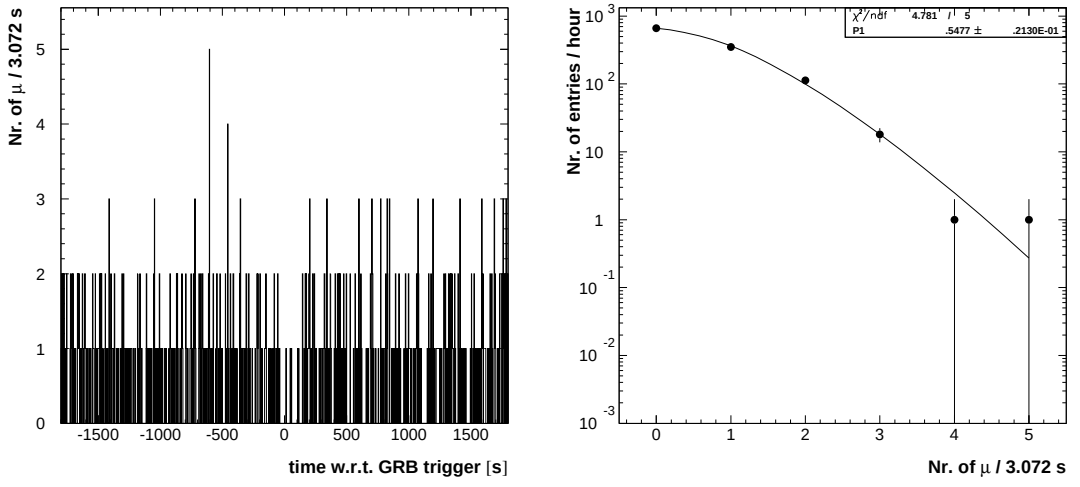

(a) (b)

Figure 8: (a) Muon rate versus time for GRB000424. (b) Corresponding distribution.

Table 2: Parameters for the optimized sampling time for all selected GRBs.

Name	Optimized sampling time ($\times$1.024 s)	Maximum muon rate/bin $r_{\max}$	Average muon rate/bin $\langle R \rangle$	$E(r \geq r_{\max} \vert \langle R \rangle)$	Upper limit 90% CL (s^{-1})	Time of maximum (s)
GRB990903	3	6	0.802$\pm$ 0.026	0.219	3.56	-1497
GRB990917	15	7	1.255$\pm$ 0.079	0.077	0.75	495
GRB991025	2	6	0.657$\pm$ 0.021	0.112	5.41	-631
GRB991103	16	16	4.961$\pm$ 0.195	0.014	1.19	-590
GRB991106	1	5	0.371$\pm$ 0.011	0.151	9.62	-238
GRB000403	5	5	0.671$\pm$ 0.032	0.457	1.86	1469
GRB000415	2	4	0.311$\pm$ 0.014	0.535	4.15	-143
GRB000424	3	5	0.548$\pm$ 0.021	0.306	3.31	-606

Table 3: Parameters for the optimized sampling time for all selected GRBs for background events.

Name	Optimized sampling time ($\times$1.024 s)	Maximum muon rate/bin $r_{\max}$	Average muon rate/bin $\langle R \rangle$	$E(r \geq r_{\max} \vert \langle R \rangle)$	Time of maximum (s)
GRB990903	6	8	0.51 $\pm$ 0.05	0.102	-4009
GRB990917	1	3	0.091$\pm$ 0.005	0.410	-3507
GRB991025	8	11	2.67 $\pm$ 0.09	0.048	-3673
GRB991103	14	14	4.07 $\pm$ 0.14	0.023	-3806
GRB991106	1	4	0.345$\pm$ 0.010	1.571	-4817
GRB000403	1	3	0.148$\pm$ 0.007	1.708	-2362
GRB000415	5	7	0.74 $\pm$ 0.04	0.009	-2570
GRB000424	5	7	1.06 $\pm$ 0.04	0.085	-1888

3.2 Lightcurve fitting

The second method used consists of the comparison of the shape of the lightcurve, as observed by BATSE, with the shape of the observed muon data. In this way we are more sensitive to multiple peak structures in the burst profile, assuming that these profiles are the same in the keV as in the TeV part of the GRB spectrum.

Lightcurve information is given for 4 energy ranges, $20 - 50$ keV, $50 - 100$ keV, $100 - 300$ keV and > 300 keV with a time resolution of 1.024 seconds and is available for 5 bursts out of the 8 that we have selected previously. An example of such a lightcurve is shown in figure 9.

The normal procedure for comparing the shape of the lightcurves with muon data would be to cross-correlate the data. However, at a timescale of 1.024 seconds the observed muonbackground rate is distributed according to a poisson function with a mean of about $\bar{\mu} = 0.3\text{muonss}^{-1}$. A standard cross-correlation method on low statistics easily results in correlation functions fluctuating from anticorrelation to correlation. Since this is not desireable we propose another method that is descibed below.

The BATSE lightcurve is normalized after the gamma-ray background is subtracted. This normalized lightcurve shape is fitted to the data from which the mean rate is subtracted. The fit parameter α can be interpreted as the number of muons contained in the lightcurve. The $\chi^2/\text{ndf} - 1$ of this fit is then compared to χ_0^2/ndf that is obtained when the muon data is fitted to a constant background only. This fit is done for every 1.024 second bin in the 1 hour period we monitor. Therefore we calculate

$$\Delta\chi^2 = \frac{\chi^2}{\text{ndf} - 1} - \frac{\chi_0^2}{\text{ndf}}, \tag{2}$$

as a function of time.

Since the lightcurve shape differs for the various energy ranges this procedure is repeated for all 4 energy ranges.

When we look at the values of $\Delta\chi^2$, shown in figures 10–14, we do not see a significant difference in any of the 4 energy ranges that could be a hint for a possible muon enhancement.

For 3 of the bursts the lightcurve shape for $E > 300$ keV could not be determined, due to low significance of the signal at this energy range. This results in a negative value for $\Delta\chi^2$.

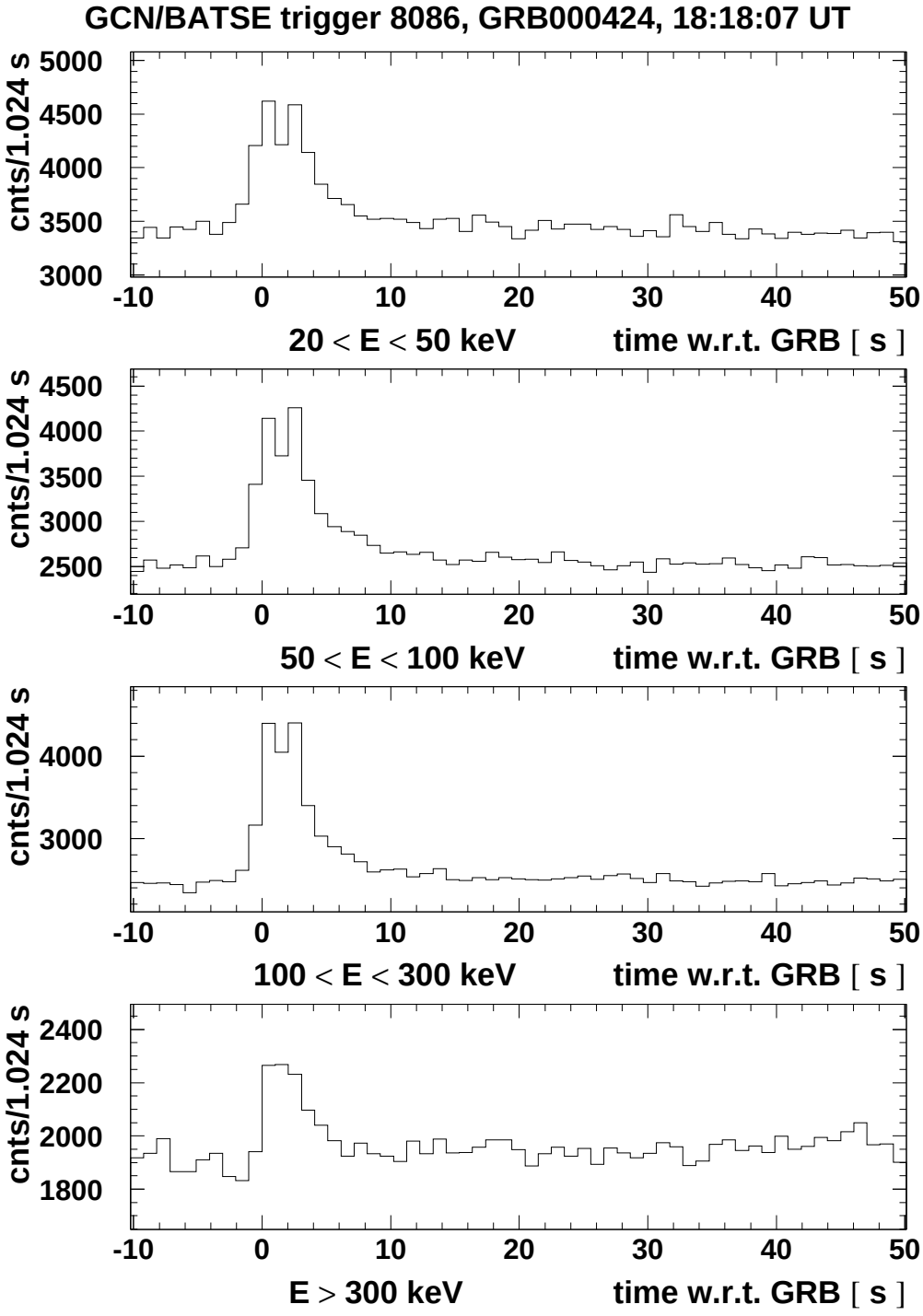

Figure 9: Lightcurve of GRB000424 measured by BATSE in four different energy ranges.

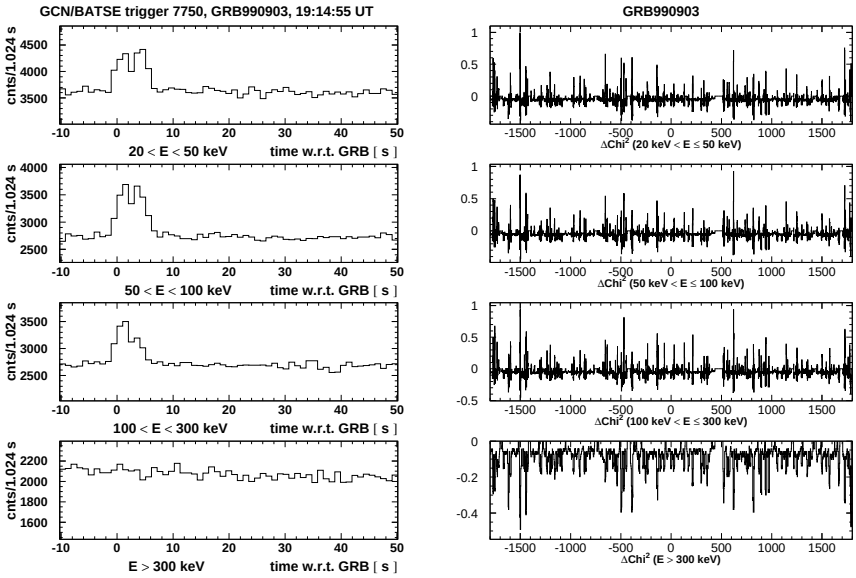

(a) (b)

Figure 10: (a) Lightcurve profile for GRB990903 as measured by BATSE. (b) $\Delta\chi^2$ for GRB990903.

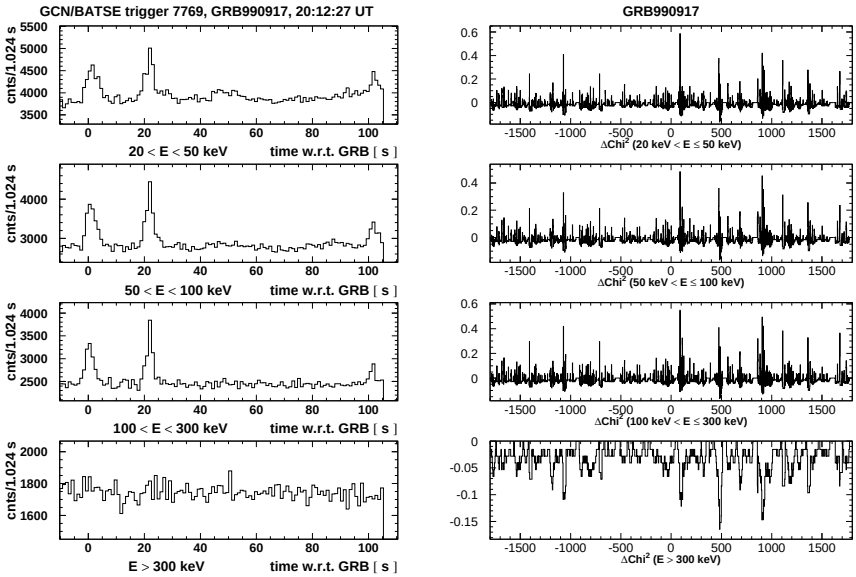

(a) (b)

Figure 11: (a) Lightcurve profile for GRB990917 as measured by BATSE. (b) $\Delta\chi^2$ for GRB990917.

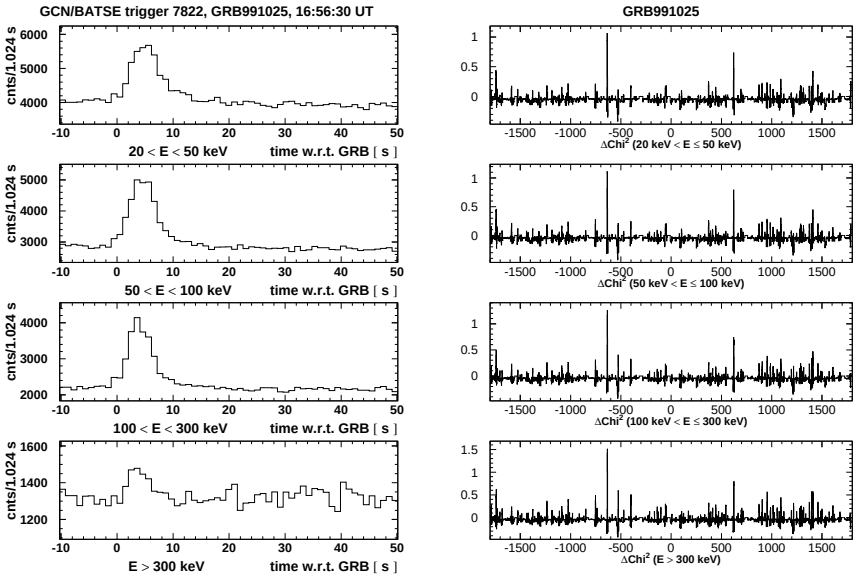

(a) (b)

Figure 12: (a) Lightcurve profile for GRB991025 as measured by BATSE. (b) $\Delta\chi^2$ for GRB991025.

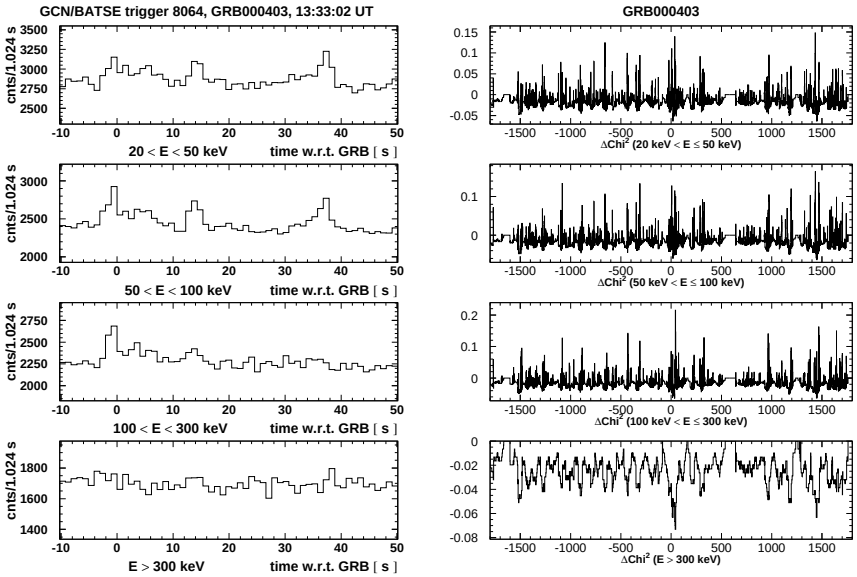

(a) (b)

Figure 13: (a) Lightcurve profile for GRB000403 as measured by BATSE. (b) $\Delta\chi^2$ for GRB000403.

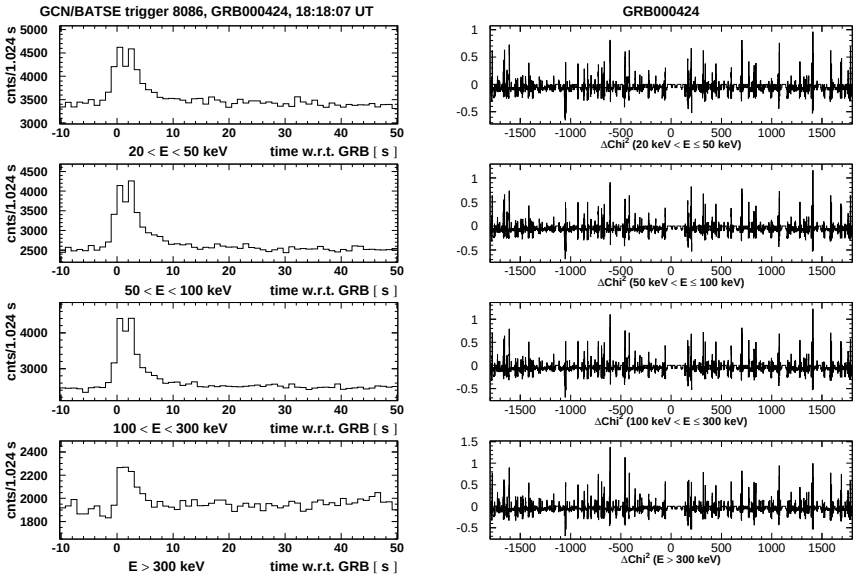

(a) (b)

Figure 14: (a) Lightcurve profile for GRB000424 as measured by BATSE. (b) $\Delta\chi^2$ for GRB000424.

3.3 24 hour scan

Complementary to the two previous methods we have searched for a GRB induced muon signal during a 24 hour period. The method is similar to the one used by J.F. Parriaud as described in [10]. We track the GRB source, starting 12 hours before the burst trigger and ending 12 hours after the trigger. The same selection criteria are used for the muon events as a function of angular position as before (see section 2.2 and 2.3).

Firstly, we look at the stability of the detector for the 24 hour period we investigate. We also look for anisotropies in the muon rate. Secondly, we look for an excess in the muon data. This is done by looking at the all sky muon rate as well as by tracking the source along the sky and comparing it with the background.

3.3.1 Stability of the detector

Before we follow the source along the sky we have to make sure that data taking conditions are stable over a 24 hour period. Therefore, we look at the rate of the selected muons and the number of scintillator hits per event versus time. We see that there are periods that the number of scintillator hits is low and periods when it is high. This high scintillator rate is caused at LEP, during beam preparation, making the muon rate go down (see figure 15). This can easily be understood because the selection of a wrong scintillator hit leads to a bad reconstruction of a track which results in a decrease of the reconstruction efficiency. Therefore, only events with a low number of scintillator hits per event (< 1.4) are selected for further analysis.

After the selection of data with low scintillator noise only 5 of the 8 selected burst periods contain enough data to proceed with this analysis.

We also look at the angular response of the detector. Therefore, we integrate the muon signal, as a function of direction in the detector, over two 12 hour periods, before and after the burst trigger, and compare the two results which are shown in figure 16.

3.3.2 Signal

In the search for a muon signal due to a GRB we first look for an excess in the all sky muon rate as a function of time. Using a binning of 2 minutes no significant excess was found during a period of 24 hours around each of the 5 bursts. The background is high, of the order of 50 muons in 2 minutes (see figure 17 for a typical example).

In order to get a better signal to noise ratio we track the source in a $5^\circ \times 5^\circ$ window.

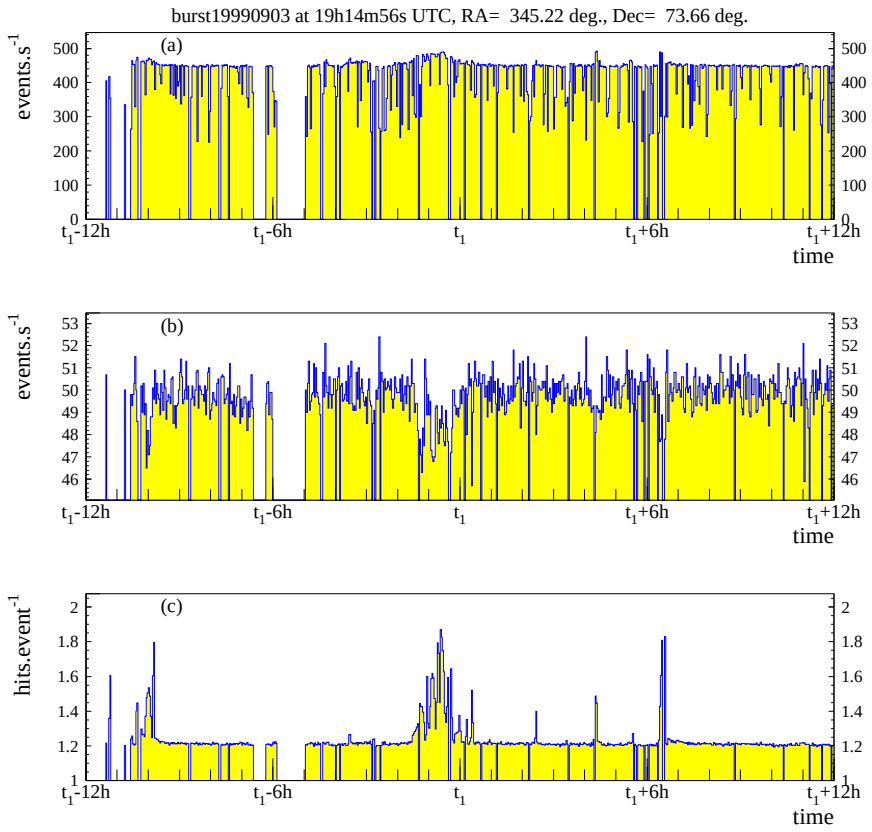

Figure 15: The effect of the number of scintillator events on the muon event rate during 24 hour around a GRB(a) Raw muon event rate. (b) Selected muon event rate. (c) Average number of scintillator hits per event. Each bin represents a 2 minute period.

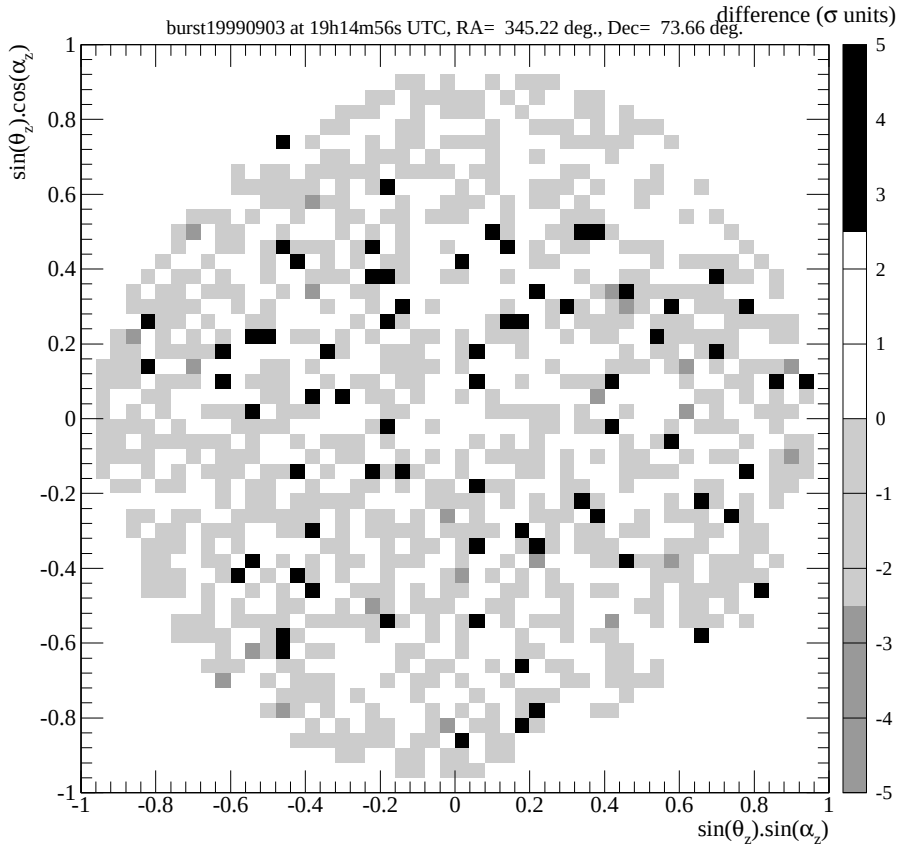

Figure 16: Difference in the muon rate before and after the GRB trigger expressed in σ in the L3+C sky.

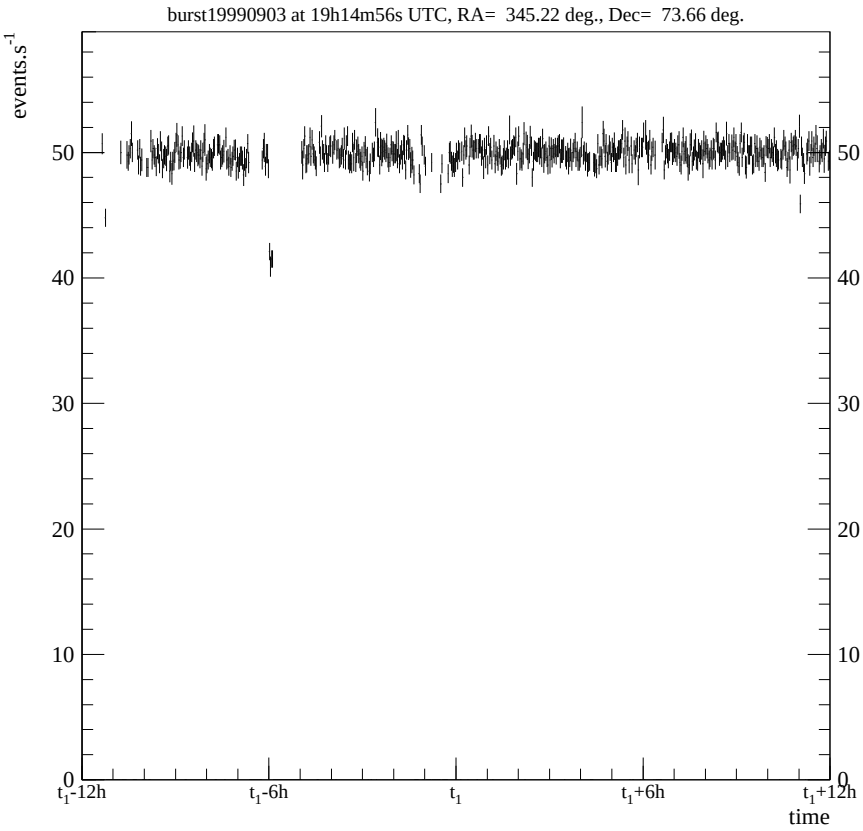

Figure 17: All sky muon rate vs. time for GRB990903.

The muon signal in this window is then compared to the background, as determined for the same directions with respect to the muon detector. To obtain the background for a fixed position relative to the detector, we average the muon rate from a $5^\circ \times 5^\circ$ window around that position during 12 hours before the burst and again for 12 hours after the burst. Both background values are compared in order to be sure that background measurement conditions are stable.

To search for an excess, the muon rate in the window around the GRB as a funtion of time is compared with the background using binning periods from 16 minutes per bin down to 1 second per bin. In figures 18 to 20 the results of this comparisson are shown for GRB990903 which has the most prominent excess of the 5 analyzed bursts. As can be seen from these figures, the difference between the signal and background stays within 3σ, so no excess was observed. For the other bursts the same conclusion applies.

For each GRB we looked at the radial distribution of the muon events integrated over azimuthal angle around the position of the GRB. For a 1 minute period around the GRB trigger time this radial distribution is monitored as a function of time. A typical example of this can be seen in figure 21. A two-dimensional representation of the events plotted in figure 21 is shown in figure 22 in which the position of the bursts corresponds to the center of the plot. None of the bursts showed a significant temporal variation near the position of the GRB within one minute of the trigger of the burst.

Finaly we look at the number of muons per unit solid angle that are observed as a function of the radial distance from the GRB position, integrated over azimuthal angle and integrated over a 24 hour period. A typical result of this is shown in figure 23. Being normalized per unit solid angle one would expect a horizontal line in case of no signal. All but one of the analyzed bursts show a radial muon distribution that corresponds to a flat distribution. We therefore can conclude that on both short (1 minute) and on long (24 hour) scale we did not see a a muon excess by looking at the radial distributions of the muons.

For GRB990903 we found a muon excess of 4.08σ around a region 1.2° from the burst location (see figure 24) which is within a 1σ uncertainty of the burst location. This could be an indication of a possible long term effect for this particular burst. Further examination of this burst is discussed in section 3.4.

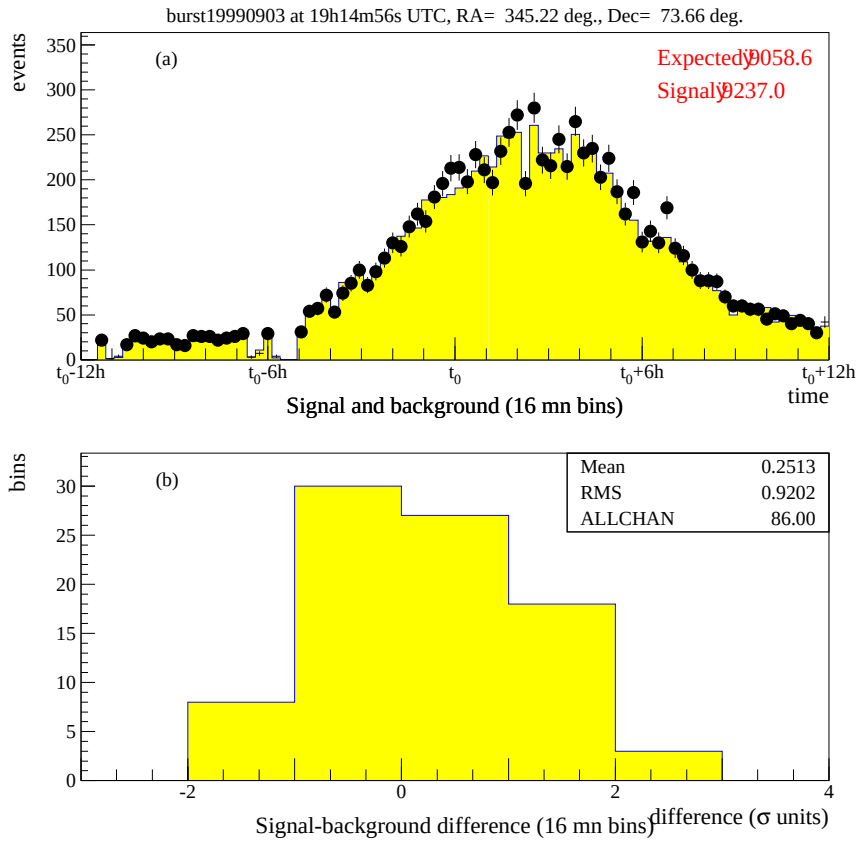

Figure 18: Signal (dots) and background muon rate for GRB990903 using 16 minute binning. (a) Number of observed events vs. time. (b) Distribution of the difference between signal and background expressed in σ units.

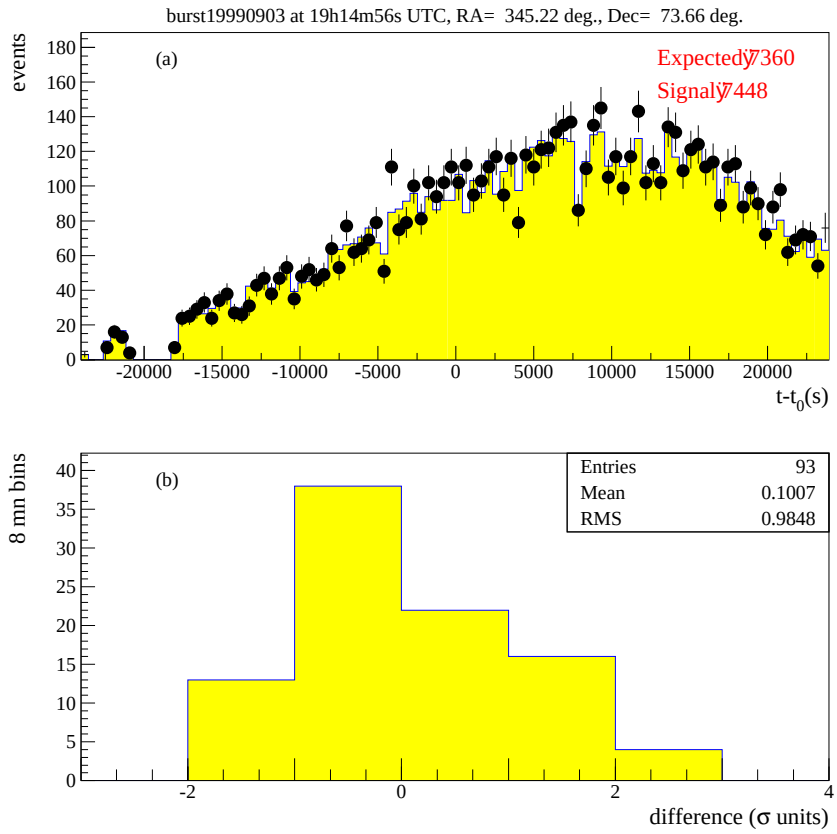

Figure 19: Signal (dots) and background muon rate for GRB990903 using 8 minute binning. (a) Number of observed events vs. time. (b) Distribution of the difference between signal and background expressed in σ units.

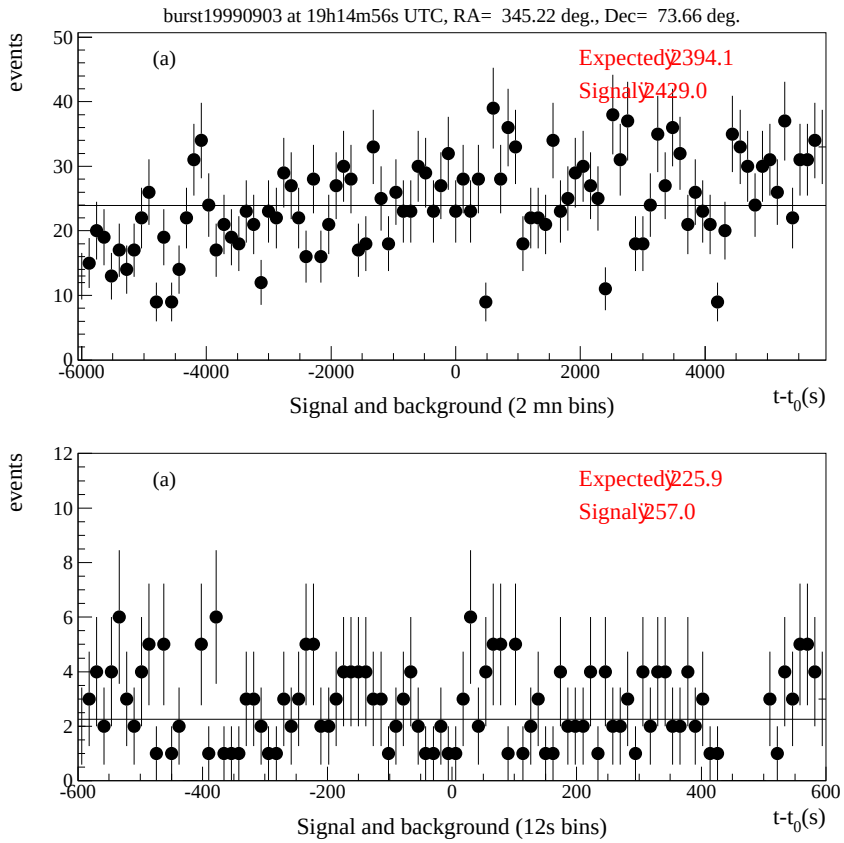

Figure 20: Signal (dots) and flat background muon rate versus time for GRB990903 using 2 minute (top) and 12 second (bottom) binning.

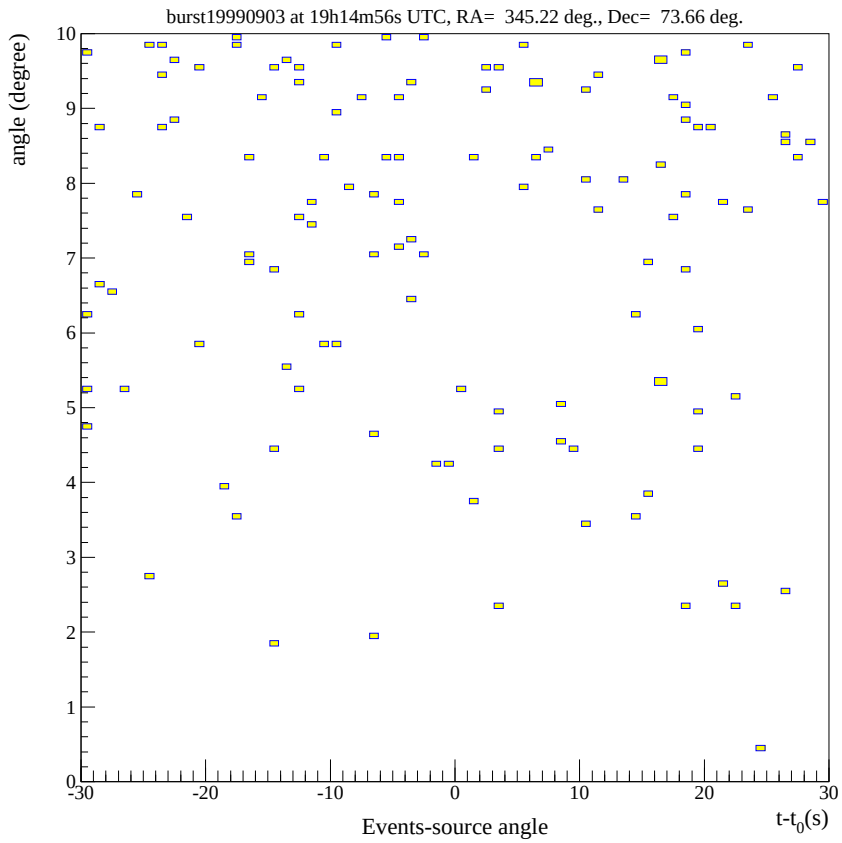

Figure 21: Radial muon distribution integrated over azimuthal angle vs. time for 1 minute around the trigger for GRB990903.

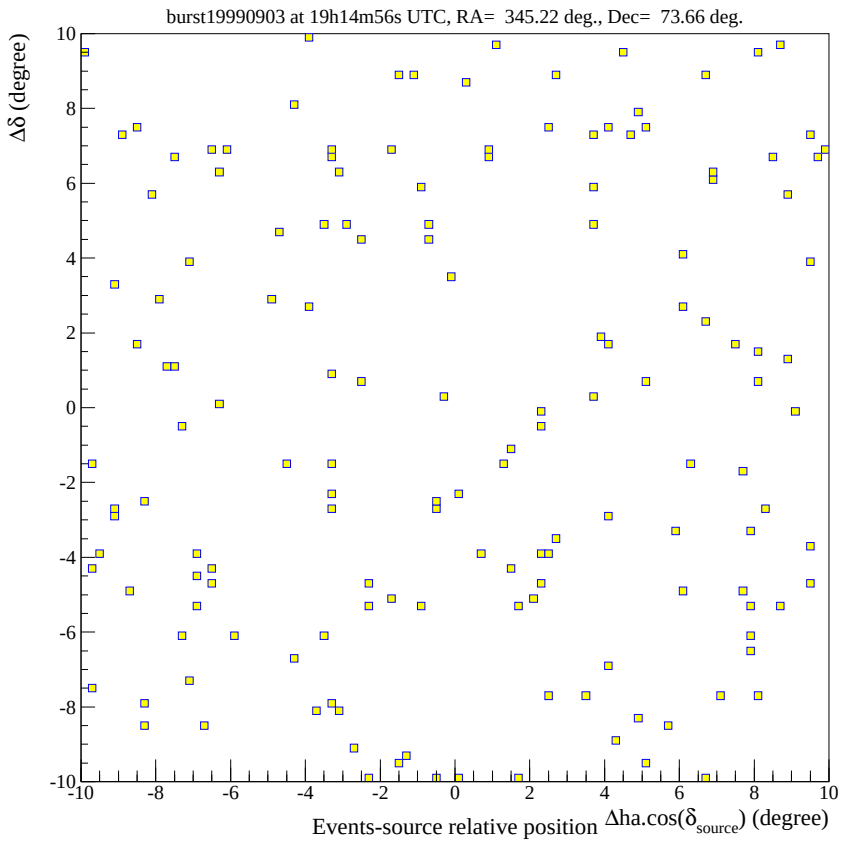

Figure 22: 2 dimensional muon distribution around the position of GRB990903 for a 1 minute period around the burst trigger.

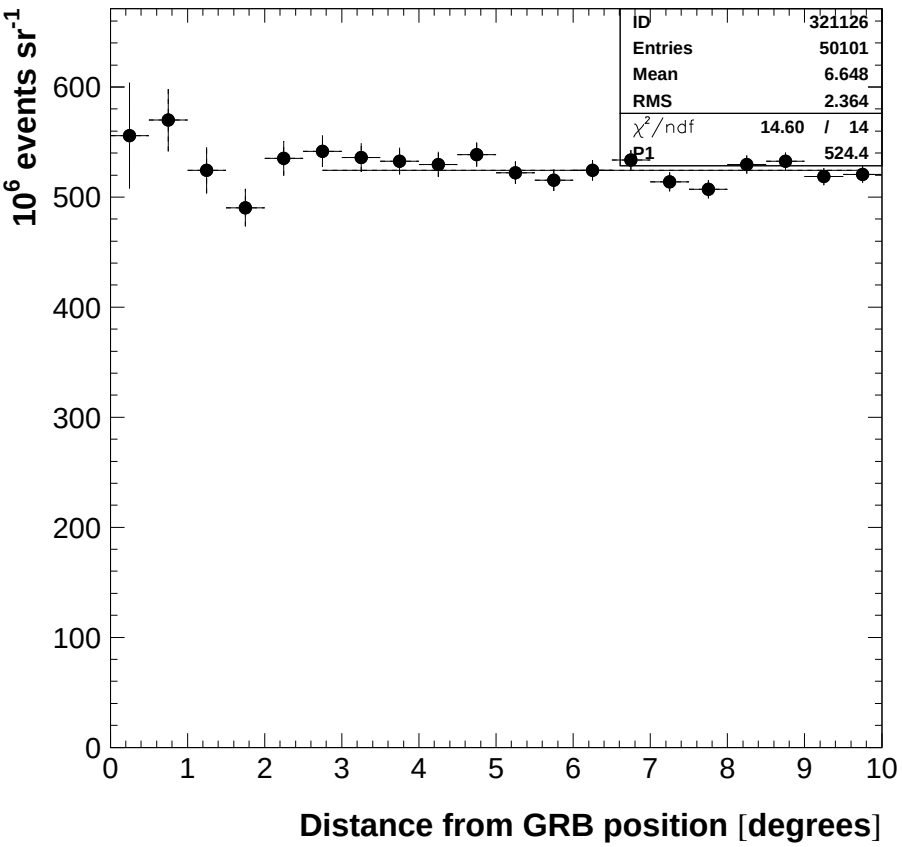

Figure 23: Number of observed muons per unit solid angle vs. radial distance integrated over azimuthal angle for GRB990917 integrated over 24 hours.

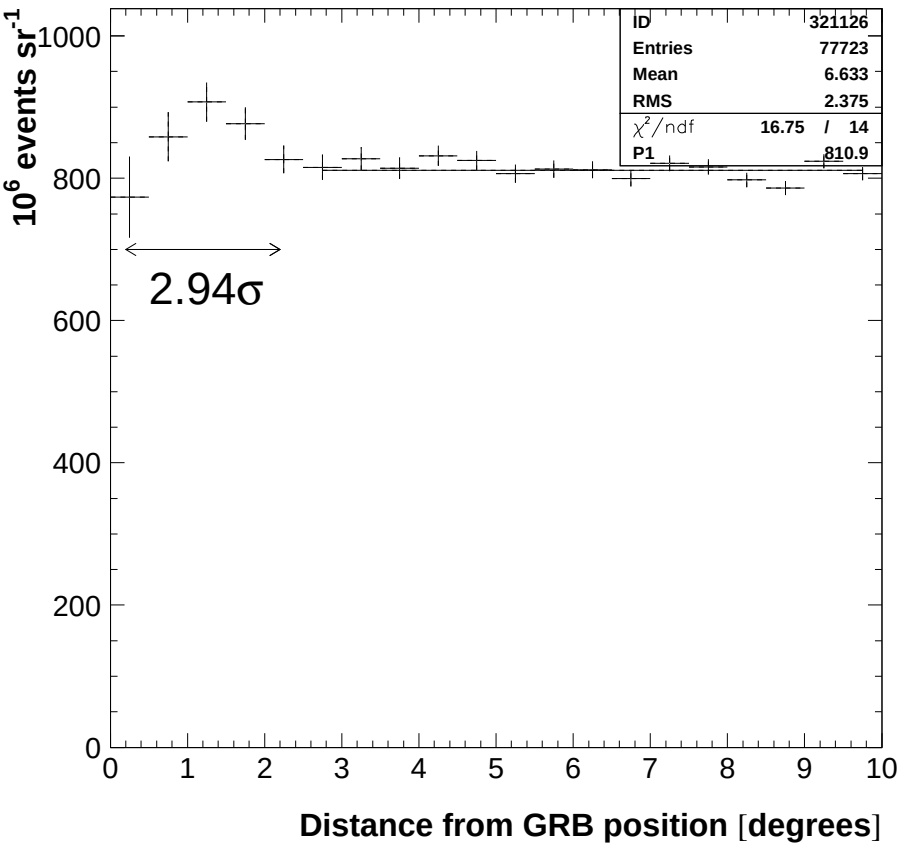

Figure 24: Number of observed muons per unit solid angle vs. radial distance integrated over azimuthal angle for GRB990903 integrated over 24 hours.

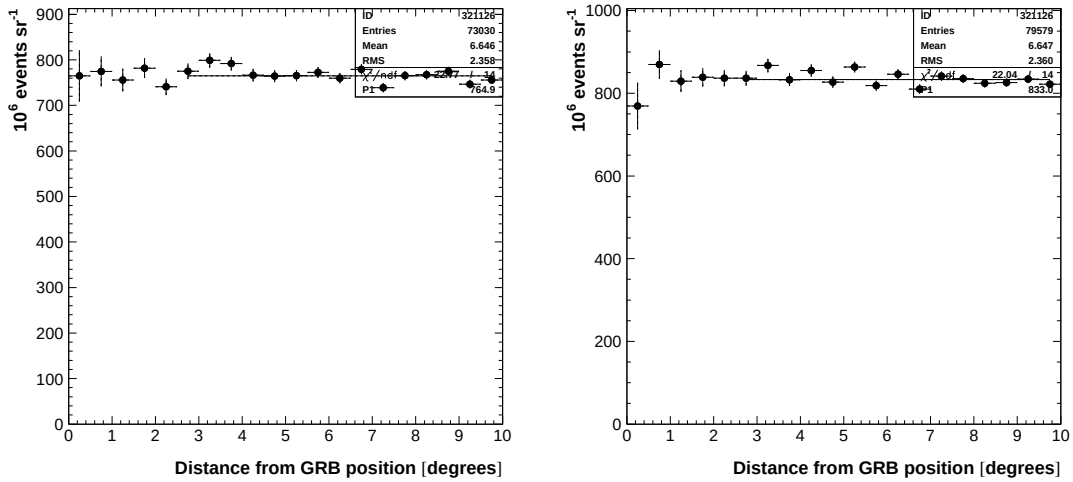

(a) (b)

Figure 25: Number of observed muons per unit solid angle vs. radial distance integrated over azimuthal angle for GRB990903 integrated over 24 hours, 1 day before the burst (a) and 1 day after the burst(b).

3.4 Closer examination of GRB990903

For GRB990903 we do a closer examination of the radial muon distribution near the burst position. Analysis of the same position of the sky 1 day before and 1 day after the burst for a period of 24 hours did not reveal a significant muon enhancement. (see figure 25). This indicates that the enhancement found integrated over 24 hours at the day of the burstis not constant in time for more than 24h.

If we look at the radial distributions using one hour periods.

Examination of the radial distribution in time intervals of one hour periods also did not show a signal. This suggests that the enhancement is created over a period of several hours instead of a short period of seconds or minutes.

Since the maximum of the enhancement found for GRB990903 is located at a distance of 1.2° from the expected position of the burst we also calculated the radial muon distribution with respect to 8 different locations surrounding the position of the GRB at a distance of 1.2° (see figure 26). Assuming that the signal would be coming from a point source near one of these locations it should show a maximum in the enhancement near 0°.

Although all of these positions show enhancements with significances between 2.7σ and 4.7σ within 2° of the center of the locations, none of these positions showed

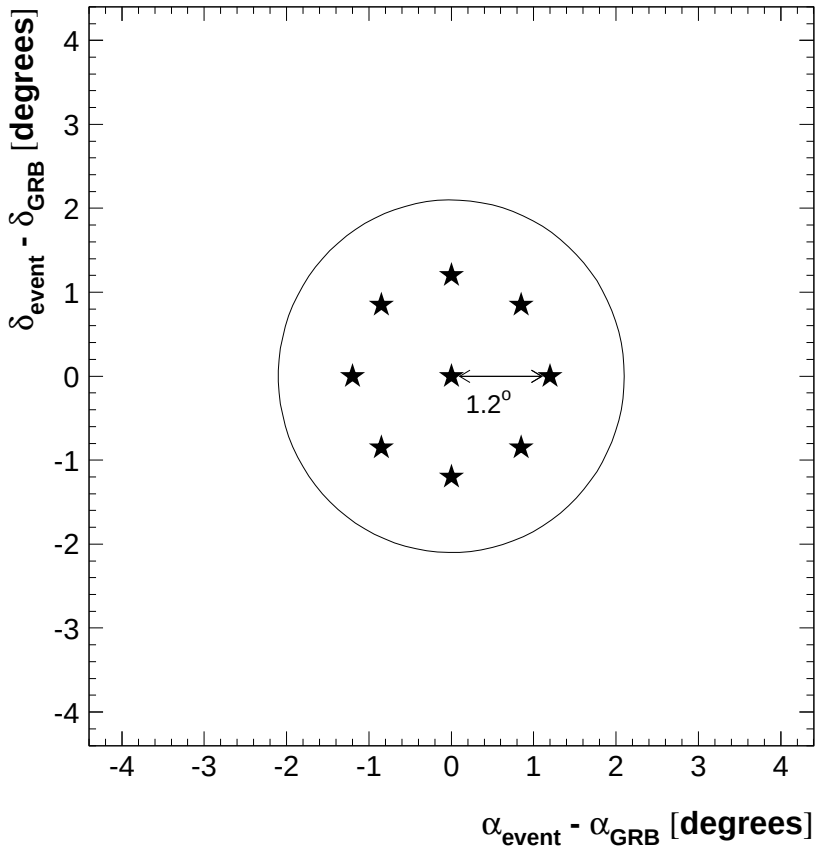

Figure 26: Locations at a distance of 1.2° around the assumed burst position of GRB990903 around which radial muon distributions are calculated.

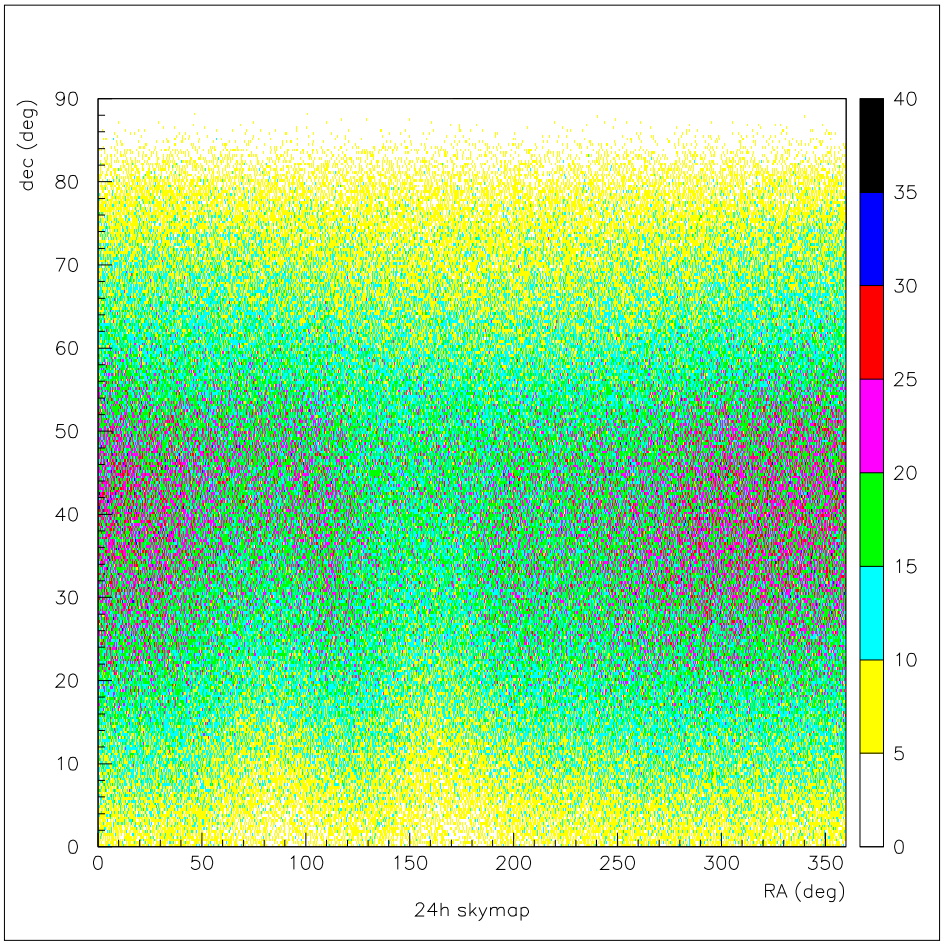

Figure 27: Muon rate distribution as a function of right ascension and declination integrated over one sidereal day around the trigger of GRB990903.

a maximum near 0°. Therefore the assumption that the enhancement in th radial distribution is coming from a point source seems to be incorrect.

Finaly, we ensure that the enhancement in the radial distribution is not caused by a point source by making a 2-dimensional map of the region surrounding GRB990903, integrated over one sidereal day. We do this by first making a map $m_\mu(\alpha, \delta)$ of the muon distribution as a function of right ascension and declination (see figure 27). From this map two profiles are derived, a declination profile $p_\delta(\delta)$ by integrating over right ascension (figure 28a) and a right ascension profile $p_\alpha(\alpha)$ by integrating over declination (figure 28b). These profiles are used to calculate the average muon rate as a function of right ascension and declination which will be used as an estimate of the muon background. The declination profile gives us the acceptance for a source

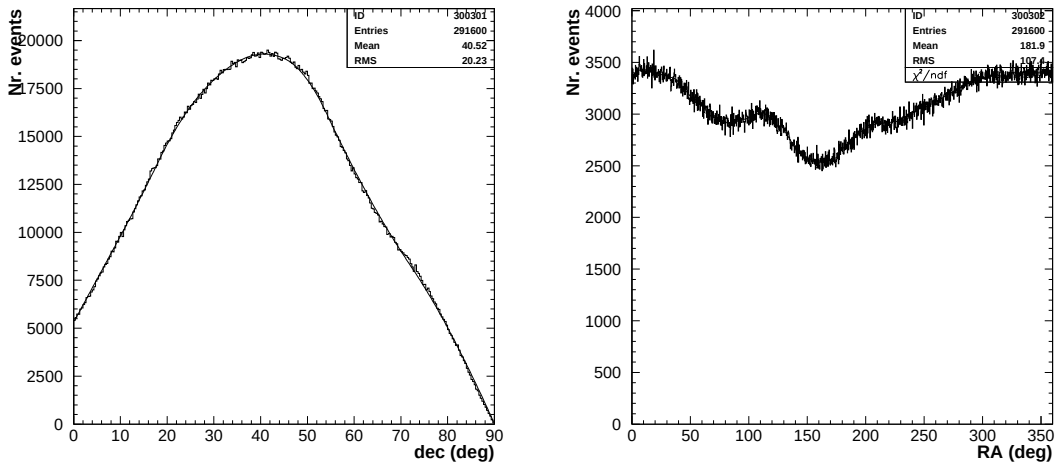

(a) (b)

Figure 28: Declination profile (a) created by integrating fig. 27 over right ascension. Right ascension profile created by integrating fig. 27 over declination.

at a certain declination combined with the effect of smaller solid angles at higher declination. The right ascension profile corresponds with the time that a source at a certain right ascension was in the field of view of the detector.

The muon background $m_{\mathrm{bg}}(\alpha, \delta)$ as a function of right ascension and declination is estimated by

$$m_{\mathrm{bg}}(\alpha, \delta) = p_{\alpha,\mathrm{norm}}(\alpha) \cdot p_{\delta}(\delta) \tag{3}$$

where $p_{\alpha,\mathrm{norm}}(\alpha)$ is the right ascension profile normalized to unity. This background and the measured muon distribution are then used to calculate the significance of the muon excess near the burst position which is shown in figure 29a. The distribution of the significance in this region is shown in figure 29b. The solid circle in the middle op the plot marks the point that are 1.2° from the location of the burst given by BATSE. The dashed line is the 1σ uncertainty of this location.

Although the estimation of background does not describe our data very well (see figure 29b) we can see that at the location of the burst there is no significant excess (figure 29a). The distribution of the significance shows a small excess in the right tail of the distribution ($\sigma > 2.5$), but these are coming from locations with high significance far from the burst position. For a good upper limit estimate a better unbderstanding of our background is needed.

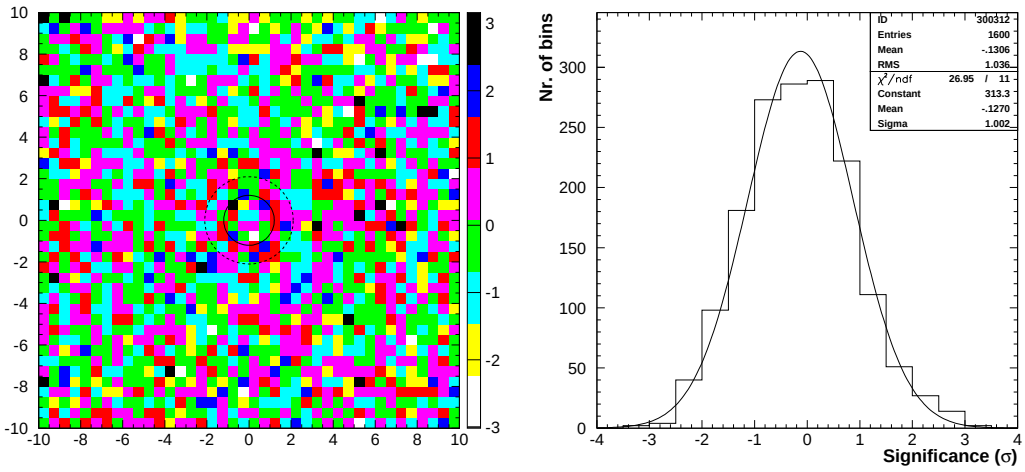

(a) (b)

Figure 29: (a) Significance of a muon excess expressed in σ near the location of GRB990903. Using a $0.5° \times 0.5°$ resolution. The location of the burst is in the center of the plot. (b) Distribution of the significance as seen in (a).

Discussion

Using the three methods described above, we did not find any direct evidence for a muon signal coming from any of the eight selected GRBs. These results can be translated into upper limits on the muon fluxes. The most sensitive method is the first one, the sampling time optimization method. Given the average muon rate and the maximum number of muons found in a bin, we use the unified approach, described in [11], to calculate the upper muon flux using a 90% confidence level.

The typical muon flux we found for the studied GRBs is $0.3\,\mathrm{m}^{-2}\,\mathrm{s}^{-1}$.

This upper muon flux can then be translated into an upper limit of the TeV gamma ray flux $\Phi_{\gamma,\mathrm{TeV}}$. From monte carlo simulations with Corsika we know that about 1% of the energy of TeV gamma-rays is converted into muons. In table 4 the results of the upper limits on the TeV gamma-ray flux are shown for each burst. From these results we get an average upper limit of the TeV gamma-ray flux of $33.6\,\mathrm{m}^{-2}\,\mathrm{s}^{-1}$.

This number can be translated into an upper limit for the luminosity of a GRB. We therefore assume that the energy is radiated away in a beam spanning 1% of the total solid angle and that we are dealing with a closeby GRB at 200 Mpc[1], which is

[1]The typical distance of a GRB is in the order of a few Gpc.

Table 4: Upper limit of the gamma-ray flux derived from the optimized sampling time method for the investigated GRBs using a 90% confidence level.

Name	$\Phi_{\gamma,\mathrm{TeV}}$ $(\mathrm{m}^{-2}\mathrm{s}^{-1})$
GRB990903	35.1
GRB990917	7.8
GRB991025	45.5
GRB991103	10.6
GRB991106	92.3
GRB000403	15.6
GRB000415	36.0
GRB000424	26.6

the typical absorption length of TeV radiation.

This results in an upper limit for the TeV gamma-ray luminosity that is given by

$$L_{\mathrm{GRB}} = 1.6 \cdot 10^{50} \left(\frac{d}{200\,\mathrm{Mpc}} \right)^2 \left(\frac{\eta}{0.01} \right) \mathrm{erg\,s}^{-1},$$

which corresponds to one percent of the total amount of the electromagnetic energy that is radiated away by a GRB.

References

[1] T. Piran. *Phys. Rep.*, 314:575–667, 1999.

[2] T. Piran. *Phys. Rep.*, 333–334:529–553, 2000.

[3] R.W. Klebesadel, I.B. Strong, and R.A. Olson. *The Astrophysical Journal*, 182:L85–L88, June 1 1973.

[4] L. Padilla et al. *Astronomy & Astrophysics*, 337:43, 1998.

[5] M. Amenimori et al. *Astronomy & Astrophysics*, 311:919–926, 1996.

[6] R. Atkins et al. *The Astrophysical Journal*, 533:L119–L122, 2000.

[7] Gamma-Ray Burst Coordinate Network web site URL: http://gcn.gsfc.nasa.gov/gcn.

[8] S.D. Barthelmy and P. Butterworth. The GCN Web Page for Real-Time GRB Information: Locations, Intensities, Fluences and Light Curves. In G.Fishman, J. Brainerd, and K. Hurley, editors, *Proceedings of the 4th Huntsville GRB Workshop*, number 428, 1998. GCN Web Site.

[9] H. Wilkens. L3 as a Muon Telescope: A search for Gamma-Ray Point Sources. Master's thesis, University of Nijmegen, 1997.

[10] J.F. Parriaud and M. Chemarin. Sun, L3+C and the 14th of July. L3+C Internal note.

[11] G.J. Feldman and R.D. Cousins. *Phys. Rev. D*, 57(7):3873–3889, 1998.